Climate Dynamics (2001) 17: 547–557

J.-L. Le Blanc · J.-P. Boulanger

Propagation and reflection of long equatorial waves in the Indian Ocean from TOPEX/POSEIDON data during the 1993–1998 period

Received: 4 October 1999 / Accepted: 22 August 2000

Abstract The present study offers a description of long equatorial wave propagation and reflection in the Indian Ocean as observed by the TOPEX/POSEIDON satellite. The equatorial longwave amplitudes are computed from January 1993 until December 1998, focusing on Kelvin (K) and first Rossby (R1) modes. The K wave is observed to propagate with a baroclinic phase speed close to 2 m/s while the R1 has a phase speed of 0.7 m/s. Wave reflections at both eastern and western boundaries are clearly observed during the entire period. At the eastern boundary K reflects into R1 with a reflection coefficient of 1.04 (reflection efficiency of 85% of that of an infinite meridional wall), and at the western boundary R1 reflects into K with a coefficient of 0.50 on average although a large seasonal and interannual variability of the reflection efficiency of the African coast is observed. Reflected K waves strongly influence the R1 variability near the western boundary as far as 60°E. Reflected R waves in turn, influence the K variability near the eastern boundary as far as 80°E. Although long equatorial waves are mainly forced by the changes in the winds during the inter-monsoon periods, reflection have a strong influence on the ocean's variability over a large part of the basin on both seasonal and interannual time scales. Focusing on the seasonal cycle of long equatorial waves (computed over 1993–1996), it is found that the constructive/destructive interaction between the wind forcing and wave reflection is responsible for the K (or R1) seasonal cycle to show a semi-annual (or annual) period near the western (or eastern) boundary. In 1994 and 1997–98, strong interannual easterlies coincident with El Niño onsets in the Pacific occurred in the Indian Ocean. Long equatorial wave propagation and reflection play a major role in creating an east–west sea level gradient along the equator, suggesting that wave dynamics and wave reflection may play a significant role in the Indian dipole mode suggested by several authors.

J.-L. Le Blanc (✉)
1-SOES, Southampton Oceanographic Centre,
University of Southampton,
Waterfront Campus, European Way,
Southampton SO14 3ZH, United Kingdom

J.-P. Boulanger
2-LODYC, UMR CNRS/IRD/UPMC,
Tour 26, Etage 4, case 100,
UPMC, 4 Place Jussieu, 75252 Paris Cedex 05,
France

1 Introduction

Indian Ocean currents are mainly driven by the monsoon winds which are characterized by two seasons, the northeast monsoon in boreal winter (December–March) and the southwest monsoon (June–September) in summer; and two inter-monsoon periods, in April–May and October–November (Fig. 1b). Winds are mainly meridional in the equatorial Indian Ocean and the zonal equatorial wind stress is weak throughout most of the year (< 0.1 N/m^2). During the transition periods, equatorial winds are westerlies. During the northeast and the southwest monsoons they are easterlies (Fig. 1b), except during the summer monsoon west of 60°E where they are westerlies because they meet the Eastern Highlands of Africa. The zonal wind signal is semi-annual over the equatorial Indian Ocean especially in the middle of the basin while it is mainly annual near the African coasts. Surface currents in the equatorial Indian Ocean are dominated by a semi-annual component and reverse direction four times a year (Tomczak and Godfrey 1994; Han et al. 1999): they flow westwards during winter and summer, and eastwards during spring and fall, the latter currents being referred to as the Wyrtki Jets (Wyrtki 1973). Equatorial waves play an important role in the adjustment of the ocean to the wind forcing.

Equatorial waves have been observed in the Indian Ocean through moored (Luyten and Roemmich 1982) and drifting buoys (Luyten et al. 1980; Reverdin et al. 1983). They also have been studied analytically through numerical modelling (O'Brien and Hurlburt 1974; Cane

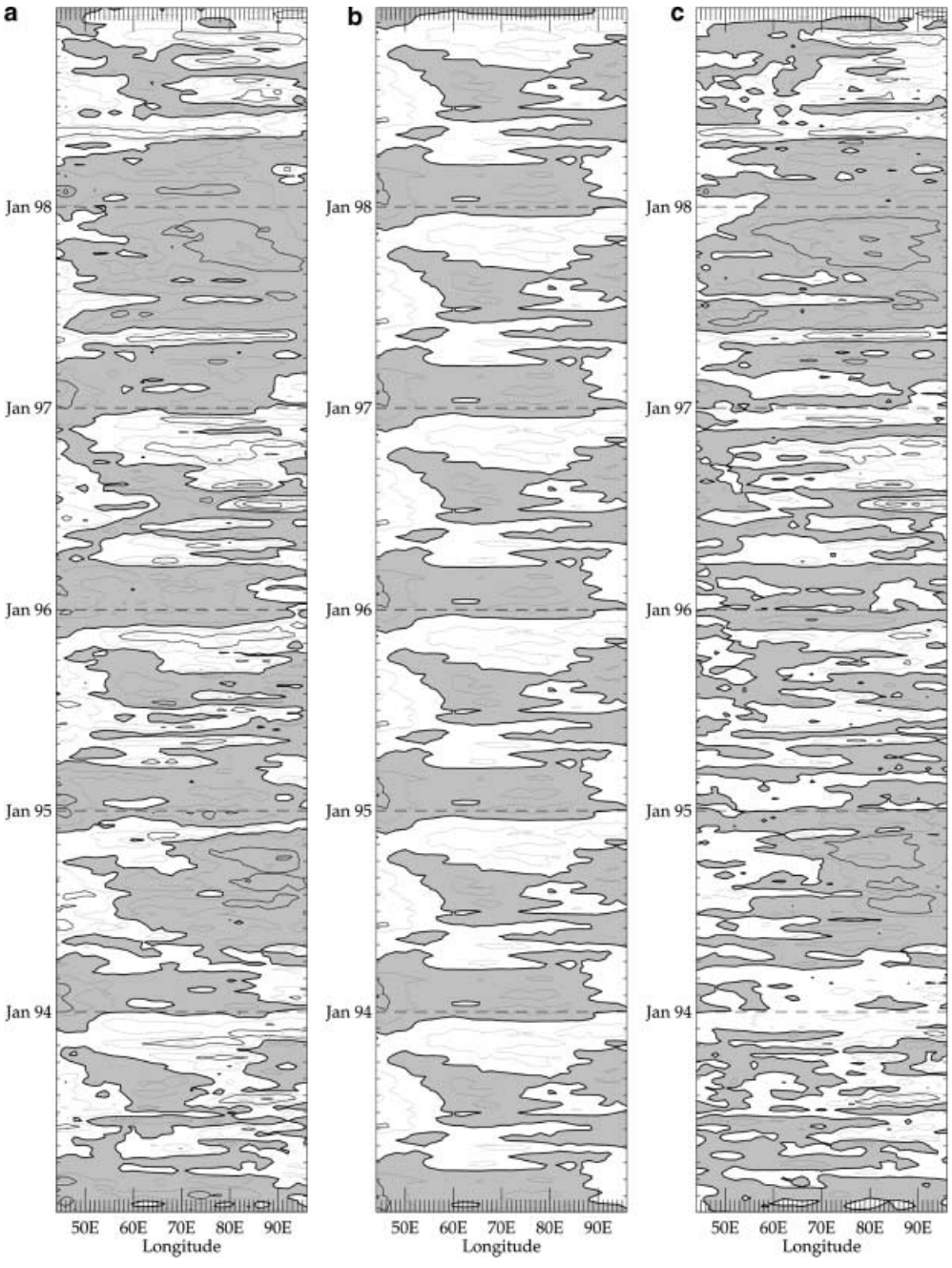

Fig. 1a–c Section between 2°N–2°S of ERS zonal wind stress of **a** anomalies relative to the 1993–1996 mean, **b** seasonal cycle computed over the 1993–1996 period with the 1993–1996 mean retrieved, and **c** interannual anomalies relative to the 1933–1996 seasonal cycle. Units are in N/m^2 and contour interval is 0.02 N/m^2. Positive (negative) coefficients are *white* (*grey*)

1980; Gent et al. 1983; Reverdin and Cane 1984; Han et al. 1999) and their effects on the coasts were studied by Clarke and Liu (1993, 1994). More recently, interannual anomalies in 1994 and 1997–1998 have motivated several studies using either observations, mainly TOPEX/POSEIDON (T/P) altimeter data (Vinayachandran et al. 1999; Chambers et al. 1999) or numerical models (Yamagata et al. 1996). Both methods show the important influence of equatorial waves on the current structure along the Indonesian west coast. In addition, recent studies of the dynamics and thermodynamics of the Indian Ocean (Webster et al. 1999; Saji et al. 1999; Anderson 1999; Reppin et al. 1999; Behera et al. 1999) seem to converge towards the existence of an intrinsic Indian Ocean dynamical mechanism, based on coupled ocean-atmosphere interactions referred to by Saji et al. (1999) as an Indian dipole mode, independent of the El Niño/Southern Oscillation (ENSO). A better understanding of the role of long equatorial waves, and their reflection on the dynamics and thermodynamics of the Indian Ocean may contribute to a more complete description of important mechanisms at work in the Indian Ocean.

In the present study, we are interested in demonstrating the existence of long equatorial wave reflection in the Indian Ocean from TOPEX/POSEIDON sea level data and in investigating their impact by focusing on the

seasonal cycle computed over the 1993–1996 period (avoiding the large variability observed in 1997–1998), and on the interannual variability (especially the 1994 and 1997–98 events). In Sect. 2, a description of data and methodology will be given. In Sect. 3, reflection at both eastern and western boundaries will be demonstrated and discussed. In Sect. 4, the seasonal cycle of both K and R1 waves will be discussed estimating the wind-forced and reflected contributions to each wave. In Sect. 5, interannual variability will be described and discussed in the light of wind-forcing and reflection. Finally, a summary and conclusions are given in Sect. 6.

2 Data and analysis methods

2.1 TOPEX/POSEIDON sea level data

The TOPEX/POSEIDON (T/P) sea level data used in the present study are provided by the Center of Space Research at the University of Texas. A detailed description of the data processing and error analysis can be found in Tapley et al. (1994). The sea level data are gridded on a 1° longitude by 1° latitude regular grid every cycle. We use the first 230 cycles covering the period January 1993–December 1998. Data are first interpolated on to a 5-day regular grid in time (i.e. with 73 time steps per year). Data are then extracted over the Indian Ocean basin (40°E–100°E/15°S–15°N). As we examine longwave propagation and reflection, the T/P sea level anomalies are first computed relative to a 4-year mean covering January 1993–December 1996. The anomalous data are then filtered in space with a 5°-longitude Hanning filter and in time with a 15-day Hanning filter. Interannual anomalies are computed relative to the 1993–1996 mean seasonal cycle.

2.2 Sea level decomposition method

The method of Boulanger and Menkes (1995) is used to project sea level data, denoted $h(x, y, t)$, into the meridional modes of long equatorial waves as follows:

$$h(x,y,t) = \sum_{0}^{N} r_n(x,t) R_n(y) \quad (1)$$

where r_n are the coefficients to be calculated by the method and R_n are longwave sea level structures (Fig. 2a; $n = 0$ refers to Kelvin wave, n greater than 0 refers to the corresponding long Rossby wave mode). The sum is assumed to be finite ($N = 20$; see Boulanger and Menkes 1995 for a discussion on the value of N). Only $n = 0$ and $n = 1$ are analyzed in the following. It should be noticed that the Kelvin and first Rossby modes have the same sign in sealevel but not in currents (Fig. 2b), i.e. a positive coefficient for the Kelvin mode represents a high sealevel (downwelling) and eastward currents while a positive coefficient for the Rossby mode represents also high sealevel (downwelling) but westward currents. Boulanger and Menkes (1995) found that these first two waves explain more than 90% of the sea level variability in a 5°N–5°S band in the Pacific. We find this result to hold for the Indian Ocean also. As for Boulanger and Menkes (1995) we consider the first baroclinic mode only.

2.3 ERS wind stress data

We use ERS-1 and ERS-2 zonal wind stress data provided by the Centre ERS d'Archivage et Traitement (CERSAT) located in the Institut Français de Recherche pour l'Exploitation de la Mer (IFREMER). The method used to convert the radar backscatter measured by the ERS-1 and ERS-2 scaterometers is described and validated in Bentamy et al. (1996). The final product used in the present study is gridded on a 1° longitude × 1° latitude regular grid and is a 7-day average wind stress field. ERS-1 data are available from August 1991 to May 1996 while ERS-2 data are available from March 1996 to December 1998. As for T/P data, ERS data are first interpolated onto a 5-day regular grid in time (i.e. 73 time steps per year). Wind stress anomalies are computed over the period January 1993–December 1996. The anomalies are then filtered in space with a 5° longitude Hanning filter and in time with a 15-days Hanning filter. Interannual anomalies are computed relative to the 1993–96 mean seasonal cycle.

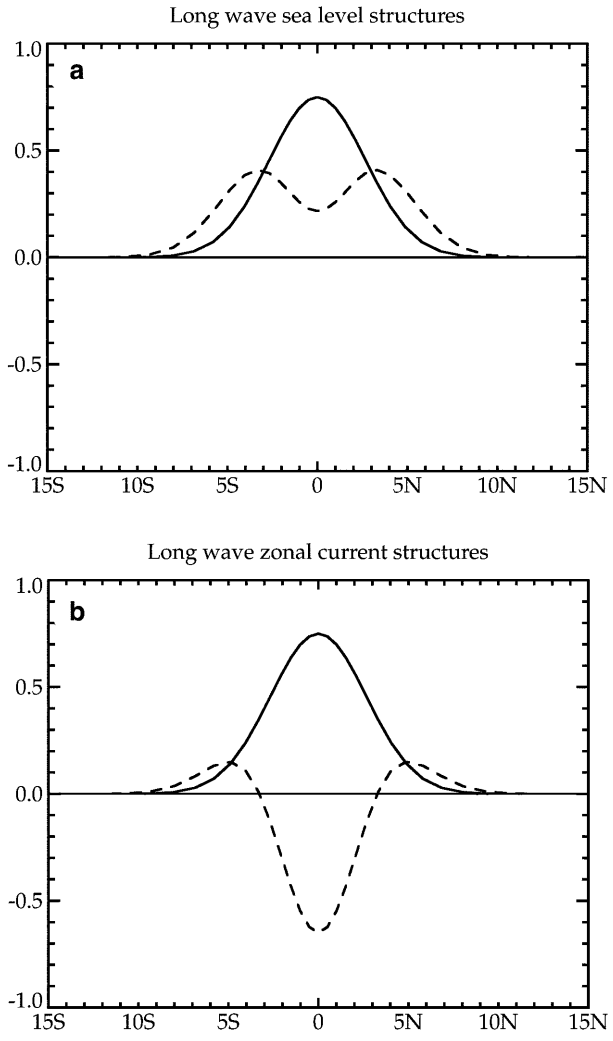

Fig. 2a, b Meridional structures of **a** sea level and **b** zonal current for Kelvin and first- Rossby modes (calculated for a 2 m/s Kelvin phase speed). Each wave amplitude at a given latitude can be obtained by multiplying the meridional structure to the calculated coefficient, yielding to cm for TOPEX/POSEIDON sea level anomaly coefficients or N/m2 for ERS wind stress anomaly coefficients

2.4 Wind decomposition method

We used the method described by Boulanger and Menkes (1995) to calculate the Kelvin and first three Rossby forcing wind coefficients. Denoting the zonal wind stress anomalies by $F(x, y, t)$, the method lies in writing first:

$$\begin{pmatrix} F(x,y,t) \\ 0 \end{pmatrix} = \sum_{0}^{N} b_n(x,t) \begin{pmatrix} R_n^u(y) \\ R_n^h(y) \end{pmatrix} \quad (2)$$

where b_n are the coefficients to be calculated by the method and $R_n^u(y)$ and $R_n^h(y)$ are respectively the longwave zonal current and sea level structures (Fig. 2). The sum is assumed to be finite ($N = 20$; see Boulanger and Menkes 1995 for a discussion on the value of N). Only b_0 and b_1 are analyzed in the following.

2.5 Wind integration along the wave characteristics

In order to estimate the wind-forced Kelvin and first-mode Rossby wave coefficients (denoted by s_n with n respectively ranging from 0 to 1), the method described by Boulanger and Fu (1996) was used. This method integrates the wind coefficients along each wave characteristic assuming zero boundary conditions as follows:

$$(\partial_t + r_{fric} + c_0\partial_x)s_0 = b_0/(\rho_0 H) \quad (3)$$

$$(\partial_t + r_{fric} - c_0/(2n+1)\partial_x)s_n = b_n/(\rho_0 H) \quad (4)$$

where r_{fric} is a Rayleigh friction coefficient (chosen to correspond to a sixmonth time scale), c_0 is the wave speed of the first baroclinic mode (2 m/s for a typical stratification in the tropical Indian Ocean), H is the thickness of the shallow-water layer (75 m), and ρ_0 is the density of seawater. This choice of parameters allows good comparison with data. Our purpose is not to make a quantitative comparison between the longwave coefficients and our simple model but rather to identify the periods and regions of major contributions of wind forcing to the observed longwave variability.

Unfortunately, as discussed in Boulanger and Menkes (1995), the wind decomposition method is not valid when the ocean basin northern or southern boundaries are close to the equator (closer than 4°N/S). As a consequence, the near-boundary wind coefficient cannot be estimated by the method. Although this may not have had a significant impact in studying long equatorial waves in the Pacific Ocean, it may affect the evaluation of the wind-forced wave amplitude in the Indian Ocean for two reasons: (1) the basin is much smaller and (2) the wind variability (especially near the African coasts) is strong (Fig. 1a). To remedy this problem, the equatorial wind variability is compared to the K and R1 wind coefficients over the central Indian Ocean. The correlation between the equatorial wind stress and the K and R1 wind coefficients is larger than 0.90 at each longitude. Thus a linear regression is computed between the wind stress and the K (or R1) wind coefficients leading to a 1.25 (or −0.60) coefficient that is relatively constant over the basin. Therefore, the method integrates the equatorial wind stress mutliplied by the appropriate coefficient over the entire Indian basin rather than the wind coefficients. We are thus able to take into account the near-boundary wind variability.

3 Long equatorial wave reflection

Figure 3 displays long equatorial K and R1 waves computed from sea level data, but with R1 inserted in between two similar K plates. The R1 plate has been horizontally reversed, i.e. the east is on the left and the west is on the right in order to show the reflecting waves as continuously eastward propagating waves.

Focusing on the eastern boundary, good coherence between the impinging K and the reflected R1 signals is observed until 80°E. Indeed comparing K and R1 coefficients at 92°E (Fig. 4a) shows that the two wave coefficients are correlated at 0.96 over the entire period. Moreover the reflection coefficient (for which the explained variance of R1 is the largest) is equal to 1.04 leading to an explained variance of 86% and a reflection efficiency of the eastern boundary of 85% of that of an infinite meridional wall. On the eastern part of the basin, K reflection strongly influences the R1 variability over the entire period, but west of 82°E, the influence of the reflection is reduced and the wind forcing is more important (Fig. 4b). At that longitude, the R1 signal starts to show a stronger semi-annual period, and the two waves are only correlated at 0.42.

At the western boundary, Fig. 3 displays also coherent signals between the two equatorial waves. Indeed, at 50°E (Fig. 4c), the wave coefficients correlate at 0.86. On average, the reflection coefficient of the western boundary (for which the explained variance of K is the largest) is 0.50. It is worth noting here that the strong variability of zonal wind near the African coasts may actually impact this estimate as it is sometimes found to be either in phase or in opposite phase with the impinging R1 signal (Figs. 1a and 3b). The value of 0.50 is therefore an estimate which will require longer time series. Moreover, it is important to underline the fact that this mean reflection coefficient actually hides a large seasonal and interannual variability of the reflection efficiency of the African coast. Indeed, Fig. 4c shows that in March–April 1993, 1995, 1996 and 1997, a large downwelling R1 wave results in a weak K wave, while in March–April 1994 and around September 1993, 1994, 1995 and 1996, a similar K wave amplitude is observed although the impinging R1 wave is of weak amplitude. Similarly, from mid-1997 to mid-1998, the K amplitude is weaker than the R1 amplitude although later the two coefficients have similar amplitudes. Various hypotheses can be suggested to explain such a large variability in the K and R1 amplitude ratio:

1. The local wind-forcing between the boundary and 50°E influences the impinging R1 wave and the generation of K wave. As will be shown in the following (see also Figs. 1a and 3b), the wind-forcing near the boundary does not have the same phase as the impinging R1 waves being thus responsible for constructive/destructive interactions.
2. The computation of the R1 wave coefficient near the African coast may be influenced by near-boundary sea level anomalies related to the intensity of the near-equatorial boundary currents known to veer eastward in summer near 3°–4°N (Philander and Delecluse 1983). This feature might be responsible for the large R1 upwelling amplitude confined near the boundary in June-August (see Fig. 5f).
3. The impinging R1 waves can interact with the Somali boundary current (usually maximum around June–July). Such an interaction has been pointed out by Philander and Delecluse (1983) who focused on the impact of the Rossby waves onto the Somali current.

It is likely that in periods of strong boundary currents, a non-linear interaction between the boundary current and the impinging wave can affect the R1 wave amplitude and its reflection. These various mechanisms should be investigated in a dynamical model in order to better understand the oceanic conditions favouring or not the reflection of Rossby waves at the African coast.

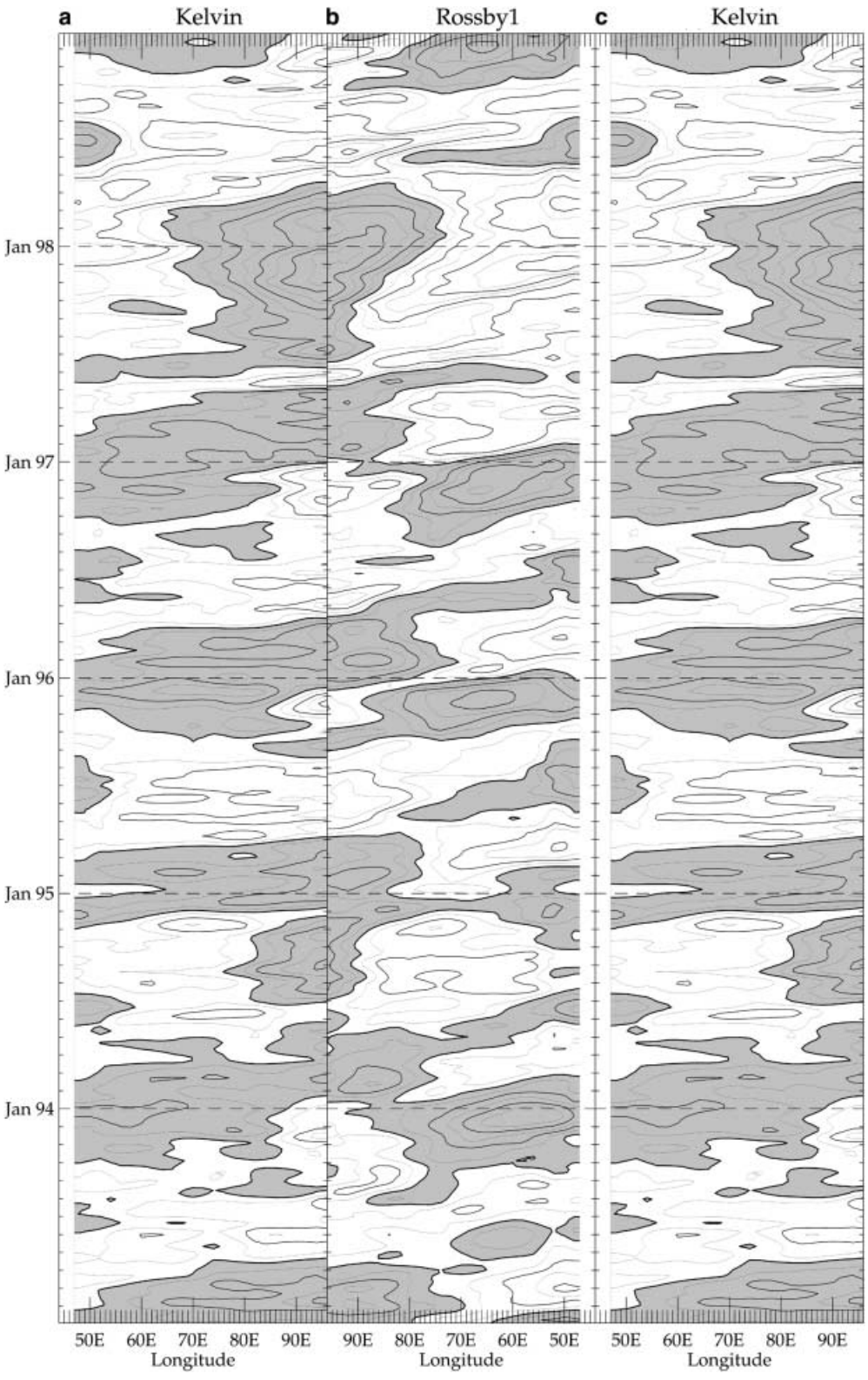

Fig. 3a Longitude-time plots of the TOPEX/POSEIDON Kelvin wave coefficient (from 44°E to 96°E), **b** the first-mode Rossby wave coefficient (in reverse display from 96°E to 44°E), and **c** the Kelvin wave coefficient (from 44°E to 96°E; repeated for comparison). Contour interval is 5 cm for both coefficients. Positive (negative) coefficients are *white* (*grey*)

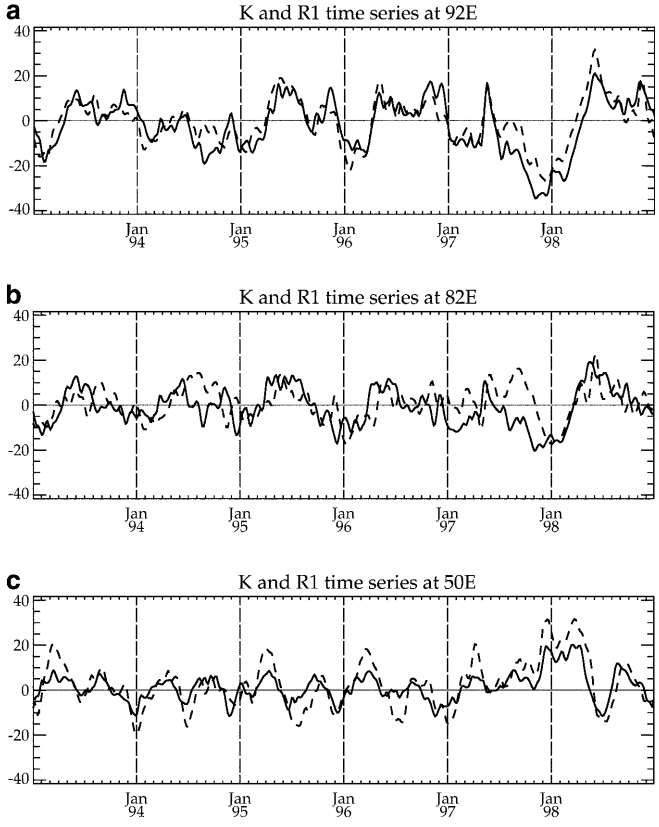

Fig. 4a Time series at 92°E of the Kelvin coefficient (*solid line*) and the first-mode Rossby coefficient lagged (backward in time) by a 10-day period corresponding to the time it takes the Kelvin wave to reach the boundary and to come back as a Rossby wave at 92°E (*dashed line*); **b** same as **a** but at 82°E and the first-mode Rossby coefficient is lagged by a 20-day period corresponding to the time it takes the Kelvin wave to reach the boundary and to come back as a Rossby wave at 82°E; **c** time series at 50°E of the Kelvin coefficient (*solid line*), the first-mode Rossby coefficient lagged (forward in time) by a 10-day period corresponding to the time it takes the Rossby wave to reach the boundary and to come back as a Kelvin wave at 50°E (*dashed line*)

4 Long equatorial wave seasonal cycle

4.1 Kelvin wave ($n = 0$) coefficient

It takes roughly one month for the K waves (at a phase speed of 2 m/s) to cross the Indian Ocean basin (approx. 6000 km). Figure 5a, b, c displays from left to right, the seasonal cycle of the wind-forcing coefficient integrated along the oceanic Kelvin wave characteristics (assuming no signal coming from the reflection at the western boundary, see Sect. 2), the seasonal cycle of the reflected component propagating freely along the K wave characteristics (the K boundary condition is the observed R1 wave at 50°E multiplied by a 0.50 reflection coefficient), and the T/P Kelvin wave seasonal cycle coefficient.

Overall, the wind-forced component (Fig. 5a) explains the major features observed in T/P (Fig. 5c). However, we can distinguish two regions: (1) The western Indian Ocean where the wind-forced signal is dominated by an annual variability although the T/P coefficients display a semi-annual variability; (2) The central and eastern Indian Ocean where the variability is mainly a blend of semi-annual and annual signals. Focusing on the first region (west of 60°E), the semi-annual variability in the T/P signal results from the reflection of R1 waves whose variability in that region is strongly semi-annual (Figs. 2 and 5f). At the western boundary, there is a clear competition between the local annual wind-forced and the semi-annual reflected components. In the rest of the domain, the wind-forcing appears to be the dominant contributor to the K wave variability.

As the 1993–1996 period is rather short to compute a seasonal cycle, even more so since it includes the 1994 event, the following climatological description is qualitative and longer time series are required to draw a more accurate description of the long equatorial wave seasonal cycle. Figure 5c displays a large upwelling amplitude from November, in the western Indian Ocean, to April in the eastern Indian Ocean. The signal is largely dominated by the wind variability although reflected waves can contribute to the November–December wave observed in the T/P coefficients but not in the wind-forcing. Despite a downwelling amplitude confined to the eastern boundary (east of 85°E) in November–December, K waves contribute to the autumn Wyrtki jet destructively in October–November over most of the basin. From April to August, the K signal in the central and eastern Indian Ocean is strongly downwelling i.e. K waves are contributing to the spring jet constructively over the entire basin. Overall, the T/P signal is semi-annual in the western Indian Ocean, and rather annual in the central Indian Ocean, and more complex near the eastern boundary.

4.2 First-mode Rossby wave coefficient

Figure 5d, e and f shows the wind-forcing coefficient integrated along the oceanic R1 wave characteristics (assuming no signal coming from the reflection at the eastern boundary), the reflected component propagating freely along the R1 wave characteristics (the R1 boundary condition is the observed K wave at 92°E multiplied by a 1.04 reflection coefficient), and the T/P first-mode Rossby wave (R1) coefficients respectively. R1 are three times slower than the Kelvin wave as suggested by longwave theory, i.e. it takes approximately three months for an R1 to cross the Indian Ocean basin from east to west.

The integrated-wind signal (Fig. 5d) is strongly semi-annual with downwelling (positive coefficients) R1 reaching the western boundary from January to April, and in autumn. Upwelling (negative coefficients) R1 can be observed from May to August, and from November to January. Although the major patterns of variability are reproduced by the wave model, large discrepancies are observed near the eastern boundary. Most of these discrepancies can actually be explained by wave reflection (Fig. 5e). Indeed, large upwelling anomalies can be

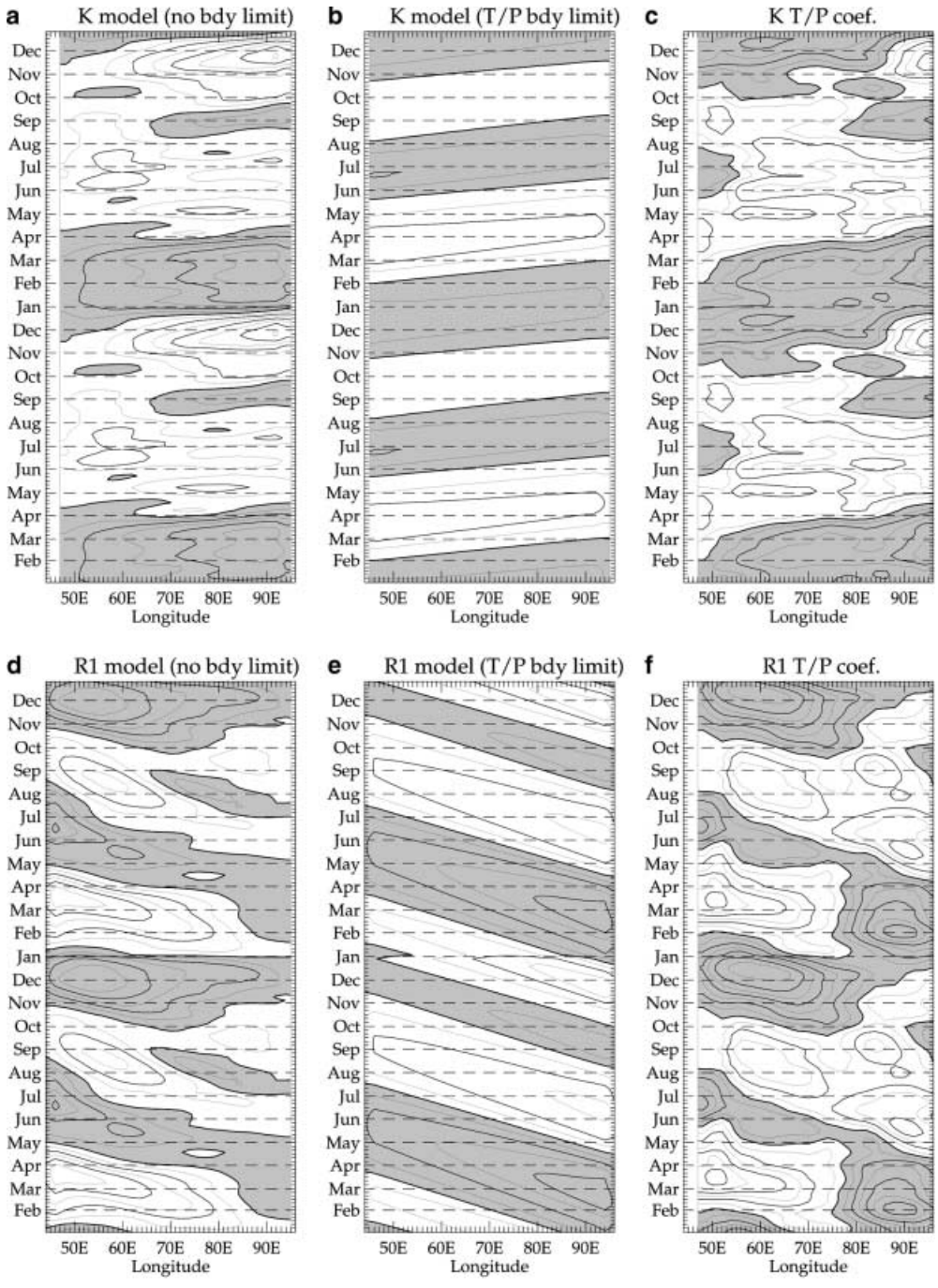

Fig. 5a–f Longitude time-plot of the seasonal cycle of **a** the ERS wind coefficient integrated along the Kelvin wave characteristics (assuming a 2 m/s baroclinic phase speed); **b** the reflected first-mode Rossby wave amplitude propagated along the Kelvin wave characteristics (assuming a 2 m/s phase speed); **c** the TOPEX/POSEIDON Kelvin coefficient; **d** same as **a** but along the first-mode Rossby wave characteristics; **e** the reflected Kelvin wave amplitude propagated along the first-mode Rossby wave characteristics (assuming a 2 m/s baroclinic phase speed); **f** same as **c** but for the first-mode Rossby wave. All coefficients are dimensionnalized (contour intervals are every 5 cm). Anomalies are computed relative to a 4-year mean (January 1993–December 1996). Positive (negative) anomalies are *white* (*grey*)

observed from January to March, and weaker upwelling ones around September. Neither is simulated by the wind variability though they are clearly observed in the T/P coefficients. Similarly, large near-boundary downwelling amplitudes can be explained by wave reflection in May–July and in November–December. Thus, depending on the period of the year, the reflected and wind-forcing signal are either in phase or in opposition of phase, and reflection is found to play a major role in explaining the observed variability east of 80°E. As a consequence of the interaction between reflected and wind-forced waves, R1 signal shows a marked dipole during most of the year (October until June). This dipole reverses sign in January–February.

5 Interannual variations

5.1 The 1994 event

In 1994, remarkable climatic conditions in the Indian Ocean were reported by several authors (Yamagata et al. 1996; Murtugudde and Busalacchi 1998; Behera et al. 1999; Reppin et al. 1999; Saji et al. 1999;

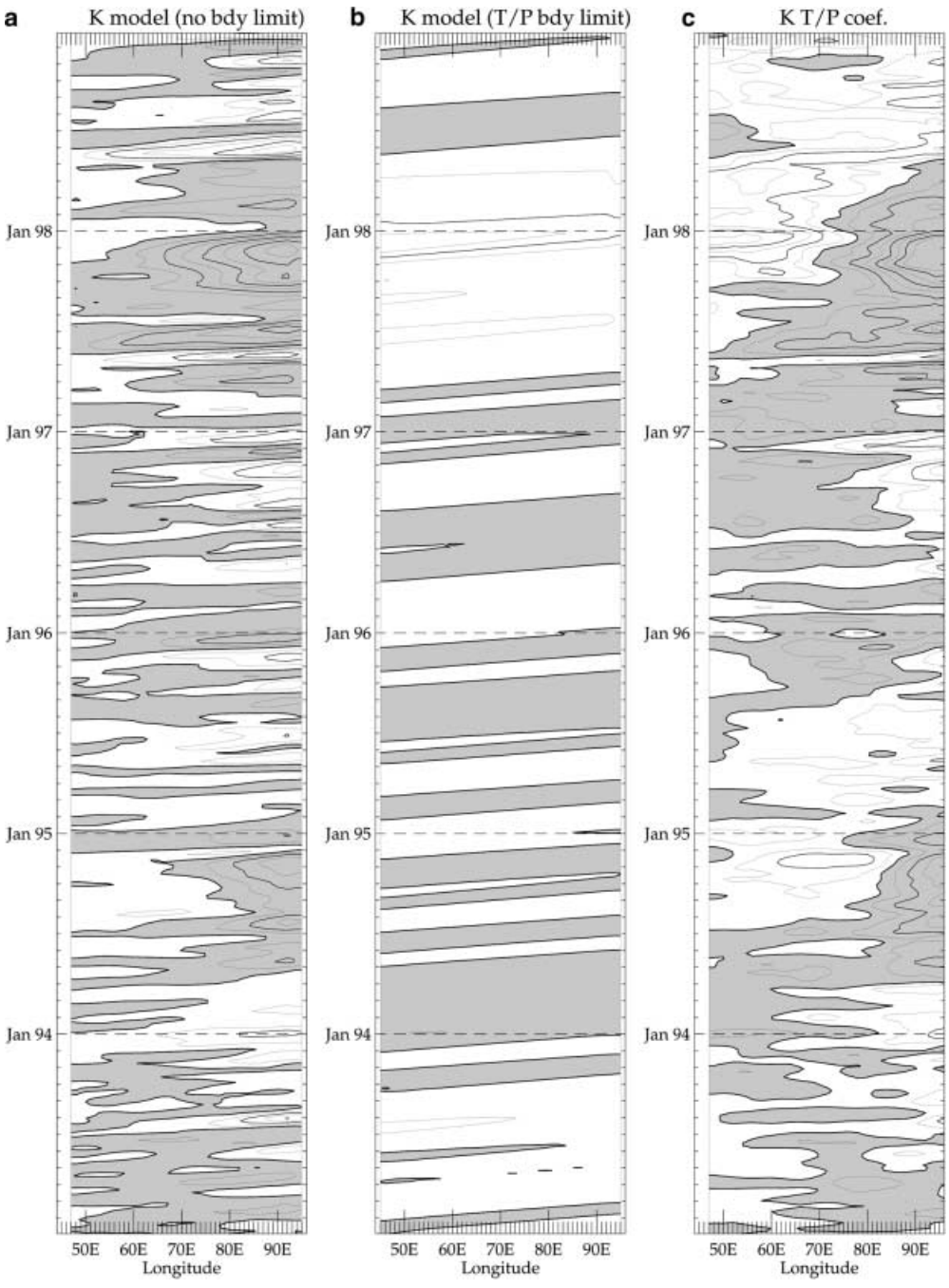

Fig. 6a–c Longitude time-plot of K interannual anomalies of **a** the ERS wind coefficient integrated along the Kelvin wave characteristics (assuming a 2 m/s baroclinic phase speed); **b** the reflected first-mode Rossby wave amplitude propagated along the Kelvin wave characteristics (assuming a 2 m/s phase speed); **c** the TOPEX/POSEIDON Kelvin coefficient. All coefficients are dimensionnalized (contour intervals are every 5 cm). Interannual anomalies are computed relative to a 4-year mean seasonal cycle (January 1993–December 1996). Positive (negative) anomalies are *white* (*grey*)

Chambers et al. 1999; Vinayachandran et al. 1999). These anomalies were observed simultaneously with weak warm anomalies in the Pacific Ocean (Boulanger and Fu 1996). Unusual westward wind anomalies were observed in the Indian Ocean east of 60–70°E from April to November 1994 (Fig. 1c). Upwelling along the coast of Java cooled the southeastern Indian Ocean and Ekman transport pushed the warm waters to the west (Vinayachandran et al. 1999; Behera et al. 1999; Chambers et al. 1999). The Wyrtki Jets were very weak in spring and autumn 1994 (Reppin et al. 1999; Vinayachandran et al. 1999).

In terms of K and R1 wave variability, Figs. 6 and 7 display similar plates to Fig. 5 but for interannual anomalies. The K coefficient (Fig. 6) is strongly dominated by the wind anomalies located east of 70°E (Fig. 1c) and generated a strong upwelling in that region. This signal was strongly reinforced by wave reflection into R1 (Fig. 7) while the wind-forcing favoured large downwelling R1 waves in the central Indian Ocean. Although this signal propagated westward, the east–west dipole signature in sea level was mainly between the central and eastern Indian Ocean. This feature contrasts with the large anomalies observed in 1997–1998.

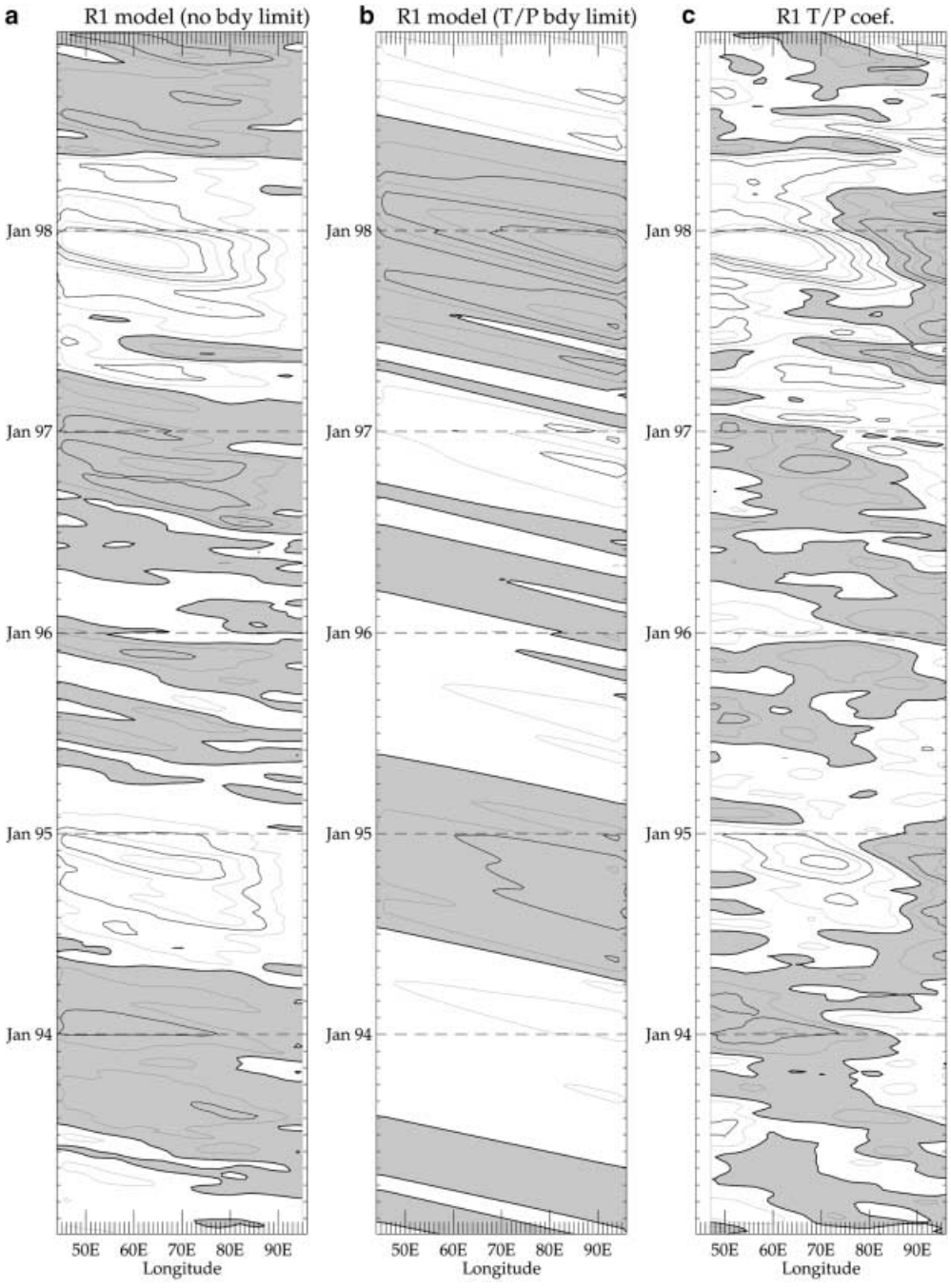

Fig. 7a–c Longitude time-plot of R1 interannual anomalies of **a** the ERS wind coefficient integrated along the first-mode Rossby wave characteristics (assuming a 2 m/s baroclinic phase speed); **b** the reflected Kelvin wave amplitude propagated along the first-mode Rossby wave characteristics (assuming a 2 m/s phase speed); **c** the TOPEX/POSEIDON first-mode Rossby wave coefficient. All coefficients are dimensionnalized (contour intervals are every 5 cm). Interannual anomalies are computed relative to a 4-year mean seasonal cycle (January 1993–December 1996). Positive (negative) anomalies are *white* (*grey*)

5.2 The 1997–1998 event

The 1997–98 El Niño is known as one of the strongest events of the century (in competition with the 1982–83 El Niño). Its effects on the Indian Ocean are therefore likely to be even larger than during the weak 1994 event. In the Indian Ocean, large, persistent easterly wind anomalies are observed over the entire basin (Fig. 1c) in May–June 1997 at a time when the eastern edge of the warm-pool in the Pacific basin had already moved eastward by more than 20° (Boulanger and Menkes 1999; Boulanger et al. submitted 2000). Whether these two features are dynamically connected is an open question. A large upwelling K wave propagated throughout the basin (Fig. 6a, c). Later the wind and wave anomalies decreased, and it was not until September 1997 that the Indian Ocean anomalies really developed with large easterly wind anomalies first located east of 70°E which then propagated westward. Simultaneously a large upwelling K signal reached the eastern boundary where it reflected reinforcing the local upwelling. The reflected R1 signal clearly influenced the wind-forced component east of 75°E (Fig. 7b). A huge R1 downwelling wave propagated westward until it reflected at the boundary. The sum of K and R1 wave signal created a large dipole signal between the eastern

and western boundaries enhancing the east–west sealevel gradient described by Webster et al. (1999) and Saji et al. (1999). Longwave reflection contributed significantly to the increase of the local sea level anomalies at each boundary. Thus they can be seen as reinforcing and potentially lengthening the anomalies in the Indian Ocean. In early 1998, the wind anomalies weakened significantly (Fig. 1c). The event terminated in April–May 1998 with the onset of the boreal summer monsoon. Saji et al. (1999) mention a seasonal phase locking as an important characteristic of the dipole mode. It may seem that the interannual anomalies develop with the onset of the boreal summer monsoon and that they last until next year's summer monsoon onset. To fully understand the processes in role in the development and termination of such interannual anomalies requires us to take into account thermodynamics within the upper-layer.

6 Summary and discussion

In this study, the propagation and reflection of long equatorial waves in the Indian Ocean have been analyzed using ERS and TOPEX/POSEIDON data from January 1993 to December 1998, and Boulanger and Menkes's (1995) decomposition method. Even though the ocean sealevel variability is more complex than can be explained by linear dynamics assuming one baroclinic mode, this method offers a powerful approach for describing long equatorial wave variability. Our analysis concerned the Kelvin (K) and the first Rossby (R1) mode. Their propagation (2 m/s for the K mode and 0.7 m/s for the R1 mode) were well monitored by the satellite.

For the seasonal cycle, their behaviour can be summarized as follows. Both K and R1 waves are triggered by the semi-annual wind reversal during the monsoon transition months in March/May and September/November. K waves have a stronger annual signal while R1 have a stronger semi-annual signal. K waves contribute positively to the Wyrtki Jet in spring and negatively in autumn, while the R1 has a slightly negative contribution in the Wyrtki Jet in spring and a positive one in autumn. Reflections at both boundaries are observed and quantified: at the eastern boundary K reflect into R1 with a reflection coefficient of 1.04 (reflection efficiency of 85% of that of an infinite meridional wall) and at the western boundary R1 reflect into K with a coefficient of 0.50 (although it is worth noting a large seasonal and interannual variability in the reflection efficiency of the African coast). Due to the small size of the Indian Ocean basin, reflected waves influence a large part of the Indian basin. At the western boundary, R1 reflect into K waves and are responsible for its near-boundary semi-annual signal. Reflections of K waves at the eastern boundary from October to May contribute to a semi-annual east-west dipole pattern in the R1 signal.

Within the period of study, two anomalous events were observed in 1994–95 and 1997–98. Both events started in April and were simultaneous with El Niño events in the Pacific. Strong easterlies in the eastern Indian Ocean induced coastal upwelling along the Indonesian coast and westward equatorial currents were observed in K and R1 signatures (negative coefficients for K and positive for R1). When both waves reached their respective boundaries the reflected waves reinforced the sealevel signal of the impinging ones. An east-west sealevel dipole was generated.

Our study confirms the fact that the Indian Ocean response to the easterly divergent winds over Indonesia in 1994–1995 and 1997–1998 is the mirror image of that in the Pacific (Chambers et al. 1999). During such events, through their propagation and reflection, both K and R1 modes contribute to amplifying the east–west sealevel gradient induced by the easterly winds; i.e. a shallow upper-layer in the east and deep in the west. Associated with that sealevel dipole, an east–west temperature dipole (cold in the east and warm in the west) has been observed. It appears to be mainly due to westward Ekman transport induced by easterlies, which push the warm waters towards the west and bring subsurface cold waters to the surface along the Indonesian coast. The K and R1 waves, by increasing the east–west sealevel gradient, are likely to contribute to this SST dipole. Further, as long equatorial K and R1 waves reflect, their zonal current signatures counteract the wind-forced zonal current signal and may then weaken and potentially reverse the westward transport of warm temperature, contributing to the termination of interannual anomalies. Therefore wave propagation and reflection are important dynamical processes in the Indian Ocean on seasonal and interannual time scales. If there are coupled modes in the Indian Ocean's variability K and R1 waves are likely to play an important role in their evolution.

Acknowledgements The research described was partially conducted for Centre National de la Recherche Scientifique at Laboratoire d'Océanographie Dynamique et de Climatologie (LODYC, Jussieu, Paris). The authors want to thank staff at the Center for Space Research at the University of Texas for providing the processed and gridded TOPEX/POSEIDON data (http://www.csr.utexas.edu/sst/gsdata.html) and those at the Center ERS d'Archivage et de Traitement located in the Institut Francais de Recherche pour l'Exploitation de la Mer for providing the processed and gridded ERS-1 and ERS-2 zonal wind stress data (http://www.ifremer.fr/cersat/ARFTP/arftp.html). The authors are grateful to Sebastien Masson for fruitful discussions and advice. Finally, they thank two anonymous reviewers whose comments helped in improving the present study.

References

Anderson D (1999) Extremes in the Indian Ocean. Nature 401: 337–339

Behera SK, Krishnan R, Yamagata T (1999) Unusual ocean-atmosphere conditions in the tropical Indian Ocean during 1994. Geophys Res Lett 26: 3001–3004

Bentamy A, Quilfen Y, Gohin F, Grima N, Lenaour M, Servain J (1996) Determination and validation of average wind fields

from ERS-1 scatterometer measurements. Global Atmos Ocean Syst 4: 1–29
Boulanger J-P, Menkes C (1995) Propagation and reflection of long equatorial waves in the Pacific Ocean during the 1992–1993 El Niño. J Geophys Res 100: 25 041–25 059
Boulanger J-P, Fu L-L (1996) Evidence of boundary reflection of Kelvin and first-mode Rossby waves from TOPEX/POSEIDON sea level data. J Geophys Res 101: 16 361–16 371
Boulanger J-P, Menkes C (1999) Long equatorial wave reflection in the Pacific Ocean during the 1992–1998 TOPEX/POSEIDON period. Clim Dyn 15: 205–225
Cane MA (1980) On the dynamics of equatorial currents, with application to the Indian Ocean. Deep Sea Res 27A: 525–544
Chambers DP, Tapley BD, Stewart RH (1999) Anomalous warming in the Indian Ocean coincident with El Niño. J Geophys Res 104: 3035–3047
Clarke AJ, Liu X (1993) Observations and dynamics of semiannual and annual sea levels near the eastern equatorial Indian Ocean boundary. J Phys Oceanog 23: 386–399
Clarke AJ, Liu X (1994) Interannual sea level in the northern and eastern Indian Ocean. J Phys Oceanog 24: 1224–1235
Gent PR, O'Neill K, Cane MA (1983) A model of the semiannual oscillation in the Equatorial Indian Ocean. J Phys Oceanog 13: 2148–2160
Han W, McCreary JP, Anderson DLT, Mariano AJ (1999) Dynamics of the eastern surface jets in the equatorial Indian Ocean. J Phys Oceanogr 29: 2191–2209
Luyten JR, Roemmich DH (1982) Equatorial currents at semiannual period in the Indian Ocean. J Phys Oceanog 12: 406–413
Luyten JR, Fieux M, Gonella J (1980) Equatorial currents in the western Indian Ocean. Science 209: 600–603
Murtugudde R, Busalacchi AJ, Beauchamp J (1998) Seasonnal to Interannual effects of the Indonesian throughflow on the tropical Indo-Pacific basin. J Geophys Res 103: 21 425–21 441
O'Brien JJ, Hurlburt HE (1974) Equatorial jet in the Indian Ocean: theory. Science 184: 1075–1077
Philander SGH, Delecluse P (1983) Coastal currents in low latitudes (with application to the Somali and El Niño currents). Deep-Sea Res 30: 887–902
Reppin J, Schott F, Fischer J, Quadfasel D (1999) Equatorial currents and transports in the upper central Indian Ocean. J Geophys Res 104: 15 495–15 514
Reverdin G, Cane MA (1984) The near surface equatorial Indian Ocean in 1979. Part 1: linear dynamics. J Phys Oceanogr 14: 1817–1828
Reverdin G, Fieux M, Gonella J, Luyten J (1983) Free drifting buoy measurements in the Indian Ocean equatorial jet. In: Nichoul JCJ Hydrodynamics of the equatorial ocean. (Ed)
Saji NH, Goswami BN, Vinyachandran PN, Yamagata T (1999) A dipole mode in the tropical Indian Ocean. Nature 401: 360–363
Tapley BD, Chambers DP, Shum CK, Eanes RJ, Ries JC (1994) Accuracy assessment of the large-scale dynamic ocean topography from TOPEX/POSEIDON altimetry. J Geophys Res 99: 24 605–24 617
Tomczak M, Godfrey JS (1994) Regional oceanography: an introduction. Pergamon, New York, pp 422
Vinayachandran PN, Saji NH, Yamagata T (1999) Response of the equatorial Indian Ocean to an unusual wind event during 1994. Geophys Res Lett 26: 1613–1616
Webster PJ, Moore AM, Loschnigg JP, Leben RR (1999) Coupled ocean-atmosphere dynamics in the Indian Ocean during 1997–98. Nature 401: 357–360
Wyrtki K (1973) An equatorial jet in the Indian Ocean. Science 181: 262–264
Yamagata T, Keizeku M, Masumoto Y (1996) Seasonal variations in the equatorial Indian Ocean and their impact on the Lombok throughflow. J Geophys Res 101: 12 465–12 473